IEEE Access
Multidisciplinary ⋮ Rapid Review ⋮ Open Access Journal

Received 17 March 2023, accepted 4 May 2023, date of publication 10 May 2023, date of current version 18 May 2023.

Digital Object Identifier 10.1109/ACCESS.2023.3274809

RESEARCH ARTICLE

A Takagi-Sugeno Fuzzy-Model-Based Tracking Framework to Regulate Heart Rhythm Dynamics

JAIRO MORENO-SÁENZ[1,2], (Member, IEEE), YING-JEN CHEN[3], (Member, IEEE), KAZUO TANAKA[1], (Fellow, IEEE), JOSÉ LUIS ARAGÓN[4], AND MARIO ALAN QUIROZ-JUÁREZ[4]

[1]Department of Mechanical and Intelligent Systems Engineering, The University of Electro-Communications, Tokyo 1828585, Japan
[2]Escuela de Ingeniería y Ciencias, Tecnológico de Monterrey, Mexico City 14380, Mexico
[3]Department of Electrical Engineering, Yuan Ze University, Taoyuan City 32003, Taiwan
[4]Centro de Física Aplicada y Tecnología Avanzada, National Autonomous University of Mexico, Queretaro 76230, Mexico

Corresponding author: Jairo Moreno-Sáenz (jairo.moreno@uec.ac.jp)

This work was supported in part by the Grant-in-Aids for Scientific Research (C) from the Ministry of Education, Science, and Culture of Japan under Grant 22K12191; and in part by Consejo Nacional de Ciencia y Tecnología (CONACyT) of Mexico under Grant CF-2023-I-1496 and Grant A1-S-8317. The work of Mario Alan Quiroz-Juárez was supported by Dirección General de Asuntos del Personal Académico (DGAPA)-National Autonomous University of Mexico under Project UNAM-PAPIIT TA101023.

ABSTRACT Arrhythmias are conditions characterized by a faster, slower, or irregular heart rhythm. Some of them may be harmless and brief, but others can lead to sudden cardiac arrest. Thus, procedures that safely restore a normal heartbeat are a matter of interest. Laboratory experiments have evidenced that some arrhythmia exhibit nonlinear deterministic behavior, which justifies the need to build mathematical models for heartbeat description. The study of these models may contribute to a better understanding of arrhythmias mechanism and new heartbeat control treatments. This paper addresses a model-based tracking control method for heart rhythm regulation in a cardiac model. Since there is no consensus on the equations describing the heart dynamics, we leverage a nonlinear oscillator that is able to reproduce a variety of electrocardiogram-like waveforms when adjusting a parameter. First of all, the nonlinear system under study is represented as a Takagi-Sugeno fuzzy model. Due to its multiple local linear systems structure, tracking control design conditions for both nominal and uncertain slave systems are formulated as linear matrix inequalities. The simulation examples show that the proposed feedback control framework can restore the heart rhythm dynamics from a non-desirable situation to the normal behavior given by the reference system, which reveals a proof of concept to use tracking control techniques to suppress pathological behaviors.

INDEX TERMS Chaotic dynamics, robust tracking control, synthetic ECG signals, Takagi-Sugeno fuzzy system.

I. INTRODUCTION

According to World Health Organization reports [1], cardiovascular diseases are the leading cause of death globally, taking an estimated 17.9 million lives each year. The term arrhythmia refers to a group of abnormalities in the heart rate or heartbeat pattern due to electrophysiological changes or congenital conditions [2]. Some of the most common arrhythmias are bradycardia, premature beats, atrial fibrillation, and ventricular tachyarrhythmias, to name but a few [3]. These last disorders may cause a sudden cardiac arrest, which can lead to death without prompt life support [4]. Treatments for arrhythmias are divided into drug and non-drug therapies, and depending on the type and severity of the irregular heartbeat, non-drug treatments can include radio-frequency ablation, electrical cardioversion, and implantable electronic devices (IEDs) [5]. IEDs, such as pacemakers and cardioverter-defibrillators, are essential to allow patients to live a normal lifestyle with their arrhythmias. A pacemaker emulates the function of the sinoatrial (SA) node, which is

The associate editor coordinating the review of this manuscript and approving it for publication was Xiaojie Su.

the natural pacemaker of the heart, by generating a periodic stimulus that helps the heart beat at a normal pace and rhythm. In contrast, cardioverter-defibrillators deliver a high-energy short-duration electric shock to restore the normal rhythm when an anomaly is detected [6]. Despite their success at saving lives, IEDs also present limitations associated with the lack of feedback, inappropriate shocks caused by an error in the diagnosis, and myocardial necrosis as a result of defibrillation [7]. In this regard, a major challenge is to optimize the way these cardiac devices operate [8]. From a dynamical system perspective, experimental studies have suggested that some arrhythmia may emerge from nonlinear deterministic dynamics (see [9], [10] and reference therein). This fact has served as the motivation to build mathematical models that describe the heartbeat dynamics at a macroscopic level [11], [12], [13], [14], [15], [16], [17], [18], which have paved the way to implement control methods to suppress pathological rhythms associated with chaotic behavior and nonlinear deterministic dynamics [19], [20].

There is a vast body of literature on control methods to deal with the regulation of cardiac rhythms. The pioneering work by Garfinkel et al. effectively stabilized a cardiac arrhythmia induced by a drug in rabbit ventricles through electrical stimulation at irregular times [21]. Later, the authors of [22] investigated a simple control to resynchronize the depolarization of the sinoatrial and atrioventricular node oscillators represented by a switching mathematical model in order to induce the faster oscillator to run slower and the slow oscillator to run faster. The approach in [23] applied an extended time-delayed feedback control method to stabilize unstable periodic orbits in a mathematical model described by a set of three-coupled modified Van der Pol oscillators. Along similar lines, Lounis et al. [24] addressed the problem of chaos control in cardiac rhythm dynamics by applying a high-order control method to a cardiac conduction model. Under this strategy, ventricular fibrillation related to chaotic behavior is converted to periodic oscillations by stabilizing unstable periodic orbits. Christini and Collins have applied chaos control to suppress a pathological nonchaotic condition (period-2 rhythm) in a cardiac model. To do so, they stabilized the model on an unstable period-1 fixed point. Additionally, they can prevent the period-doubling bifurcation into alternans by tracking the 1-period rhythm in its unstable regime [25]. Boroujeni et al. [26] presented a nonlinear spatio-temporal delayed feedback control strategy to stabilize alternans of cardiac tissue modeled by a nonlinear partial difference equation. Recent works have considered multivariable control (MIMO) schemes, for instance, the proposal in [27] synchronized two identical non-autonomous nonlinear oscillators, represented in both integer-order and fractional-order forms, via an adaptive control law, while the research in [28] utilizes an observer-based smooth sliding mode controller to regulate the heart rate with bradycardia. A novel neural network-based backstepping approach to achieve pacing-rate control, with the potential for dual-sensor pacemaker applications, was given in [29]. Reference [30] covered the regulation of heartbeat fluctuations with a fuzzy fractional-order proportional-integral-derivative controller for a pacemaker. A similar work has been proposed in [31], whose main approach is to design a fractional-order PID controller through a particle swarm optimization algorithm for a cardiac pacemaker model in order to regulate the heart rate of a pathological condition. Lastly, other efforts consider the combination of fuzzy logic and conventional PID control to design fuzzy proportional-integral-derivative (FPID) controllers which allow determining the pacing rate of cardiac pacemakers in order to achieve matches between real and desired heart rates [32]. All of these works have notably contributed to the application of control techniques to the regulation of heart rhythm and rate. Nevertheless, these problems remain a challenge from both the medical and engineering perspectives. This work focuses on the design of a multivariable feedback controller for the tracking problem of a nonlinear oscillator in a master-slave framework. Both master and slave systems will make use of a Takagi-Sugeno fuzzy representation of the dynamical model introduced in [33], which is capable to generate a range of electrocardiogram (ECG) waveforms when varying an intrinsic parameter of the system. Since the core of the Takagi-Sugeno fuzzy is a multiple linear systems structure, design conditions will be expressed in terms of linear matrix inequalities (LMI), which can be efficiently solved by semidefinite programming tools. The first approach in this article will tackle the tracking problem of two ECG oscillators, where a parallel distributed compensation (also known as PDC) law is used to cancel the mismatching term between the pair of models and stabilize the error dynamics. On the other hand, the novelty of the second approach is to consider a parametric uncertainty in the intrinsic parameter that allows generating a variety of ECG signals, and the tracking control objective is achieved by a robust control strategy alongside the feedback stabilization of the reference model. The two approaches assume that the master and slave systems are equipped with different membership functions and the discrepancy brought by them will be mitigated in a $\mathcal{L}_2$-norm fashion.

The main contributions of this work are listed as follows.

- Representation of an ECG nonlinear oscillator as a Takagi-Sugeno fuzzy model. To the best of our knowledge, the analysis of nonlinear oscillators representing cardiac dynamics has not been performed using the model-based fuzzy control.
- Implementation of a chaos control method to avoid pathological heart rhythm. Undesirable behaviors are suppressed by introducing a multivariable feedback controller for the tracking problem of a nonlinear oscillator in a master-slave framework. The fact that a variation on a parameter of the model is responsible for having normal or abnormal dynamical behaviors motivates the use of a robust tracking scheme.
- Formulation of novel control design conditions for the robust tracking control of an uncertain slave system.

The multiple linear subsystems structure of the Takagi-Sugeno fuzzy model lets us formulate the conditions as LMI expressions, which can be efficiently solved by a variety of toolboxes.
- Presentation of a conceptual proof that could assist in the improvement of cardiac devices by showing that it is possible to avoid the onset of pathological heart rhythms through the implementation of chaos control methods.

After this introduction, the paper will be structured in the following manner. Section II will discuss the mathematical background for this research. Then, the construction of the Takagi-Sugeno fuzzy model of the ECG nonlinear oscillator will be given in Section III. LMI conditions for the tracking problem and the robust scheme control of the uncertain ECG system will be derived in Section IV and V, respectively. Both sections will give simulation results to validate the proposed framework.

II. BACKGROUND

In the present section, we will briefly summarize the necessary background for this work. As for our setting, bold letters will be read as matrices and vectors, and scalars otherwise. Moreover, the standard notation will be used for operations. Although the state variables $\boldsymbol{x}(t)$, control input vector $\boldsymbol{u}(t)$, output $y(t)$, and disturbance $w(t)$ depend on time, we will omit their time dependence for the sake of ease.

A. TAKAGI-SUGENO FUZZY REPRESENTATION

Consider a nonlinear system with an external bounded disturbance w of the form

$$\begin{cases} \dot{\boldsymbol{x}} = \boldsymbol{f}(\boldsymbol{x}) + \boldsymbol{g}(\boldsymbol{x})\boldsymbol{u} + \boldsymbol{m}(\boldsymbol{x})w, \\ y = k(\boldsymbol{x}), \end{cases} \tag{1}$$

where $\boldsymbol{x} = [x_1,\ x_2,\ \cdots, x_n]^T$ is the state vector, $\boldsymbol{u} \in \mathbb{R}^{n\times 1}$ is the control input vector, y is the output, $\boldsymbol{f}(\boldsymbol{x}) \in \mathbb{R}^{n\times 1}$, $\boldsymbol{g}(\boldsymbol{x}) \in \mathbb{R}^{n\times n}$ and $\boldsymbol{m}(\boldsymbol{x}) \in \mathbb{R}^{n\times 1}$ are vector-valued functions and $k(\boldsymbol{x})$ is a scalar function. The application of the sector nonlinearity approach [34] leads to the following Takagi-Sugeno fuzzy model

$$\begin{cases} \dot{\boldsymbol{x}} = \sum_{i=1}^{z_r} h_i(\boldsymbol{x})\{\boldsymbol{A}_i\boldsymbol{x} + \boldsymbol{B}_i\boldsymbol{u} + \boldsymbol{E}_i w\}, \\ y = \sum_{i=1}^{z_r} h_i(\boldsymbol{x})\boldsymbol{C}_i\boldsymbol{x}. \end{cases}$$

Clearly, the previous equation is a blending of z_r linear systems weighted by the membership functions $h_i(\boldsymbol{x})$ which are non-negative and satisfy the property $\sum_{i=1}^{z_r} h_i(\boldsymbol{x}) = 1$. Therefore, $\boldsymbol{A}_i \in \mathbb{R}^{n\times n}$ are the state matrices, $\boldsymbol{B}_i \in \mathbb{R}^{n\times 1}$ are the input matrices, $\boldsymbol{E}_i \in \mathbb{R}^{n\times 1}$ are the disturbance input matrices and $\boldsymbol{C}_i \in \mathbb{R}^{1\times n}$ are the output matrices. For more details on the theoretical foundations of Takagi-Sugeno fuzzy models, we refer readers to [35].

B. DISTURBANCE ATTENUATION

A method to measure the effect of an external disturbance on the dynamics of the system (1) is by using the $\mathcal{L}_2$-norm defined as

$$\int_0^{t_f} k(\boldsymbol{x})^T k(\boldsymbol{x})dt \le \gamma^2 \int_0^{t_f} w^T w dt.$$

Here, $\gamma > 0$ is the attenuation factor and t_f denotes the final time. The system meets the $\mathcal{L}_2$-norm if the following inequality holds true.

$$-\dot{V}(\boldsymbol{x}) - k(\boldsymbol{x})^T k(\boldsymbol{x}) + \gamma^2 w^T w \ge 0,$$

where $V(\boldsymbol{x}) : \mathbb{R}^n \to \mathbb{R}$ becomes a Lyapunov function for the system.

C. SCHUR COMPLEMENT

Let $\boldsymbol{L}$, $\boldsymbol{M}$ and $\boldsymbol{N} > \boldsymbol{0}$ be matrices of appropriate sizes. The inequality $\boldsymbol{L} - \boldsymbol{M}^T\boldsymbol{N}\boldsymbol{M} > \boldsymbol{0}$ is equivalent to

$$\begin{bmatrix} \boldsymbol{L} & \boldsymbol{M}^T \\ \boldsymbol{M} & \boldsymbol{N}^{-1} \end{bmatrix} > \boldsymbol{0},$$

and vice versa [36].

D. YOUNG'S INEQUALITY

Let $\boldsymbol{M}$ and $\boldsymbol{N}$ be matrices of appropriate sizes. From the inequality $(\boldsymbol{M}_1 - \boldsymbol{N}_1)^T(\boldsymbol{M}_1 - \boldsymbol{N}_1) + (\boldsymbol{M}_2 - \boldsymbol{N}_2)^T(\boldsymbol{M}_2 - \boldsymbol{N}_2) \ge \boldsymbol{0}$, it can be concluded that

$$\begin{aligned} \boldsymbol{M}_1^T\boldsymbol{M}_1 + \boldsymbol{N}_1^T\boldsymbol{N}_1 + \boldsymbol{M}_2^T\boldsymbol{M}_2 + \boldsymbol{N}_2^T\boldsymbol{N}_2 \\ \ge \boldsymbol{M}_1^T\boldsymbol{N}_1 + \boldsymbol{N}_1^T\boldsymbol{M}_1 + \boldsymbol{M}_2^T\boldsymbol{N}_2 + \boldsymbol{N}_2^T\boldsymbol{M}_2, \end{aligned}$$

which is a reformulation of Young's inequality [37].

III. TAKAGI-SUGENO FUZZY REPRESENTATION OF THE ECG NONLINEAR OSCILLATOR

This section deals with the construction of a Takagi-Sugeno fuzzy model representation of the ECG nonlinear oscillator proposed in [33], whose output resembles electrocardiogram waveforms corresponding to both normal heartbeat and a variety of arrhythmias. Firstly, consider the following fourth-order unforced nonlinear system

$$\begin{aligned} \dot{x}_1 &= \tau\left(x_1 - x_2 - \zeta x_1 x_2 - x_1 x_2^2\right), \\ \dot{x}_2 &= \tau\left(\eta x_1 - 3x_2 + \zeta x_1 x_2 + x_1 x_2^2 + \beta(x_4 - x_2)\right), \\ \dot{x}_3 &= \tau\left(x_3 - x_4 - \zeta x_3 x_4 - x_3 x_4^2\right), \\ \dot{x}_4 &= \tau\left(\eta x_3 - 3x_4 + \zeta x_3 x_4 + x_3 x_4^2 + 2\beta(x_2 - x_4)\right). \end{aligned} \tag{2}$$

Here, the former pair of equations can be thought of as a model of the sinoatrial (SA) node, which is the heart's natural pacemaker. In contrast, the latter pair of equations are related to the dynamics of the atrioventricular (AV) node. Throughout this paper, we will use the scale factor $\tau = 7$ which corresponds to a normal heartbeat of approximately 80 beats per second [33]. By setting $\zeta = 1.35$ and $\beta = 4$, the variation of the parameter η leads to the generation of a variety of ECG-like signals, which are the linear combination of the states given by $y_{ECG} = \boldsymbol{C}\boldsymbol{x}$, where $\boldsymbol{x} = [x_1\ x_2\ x_3\ x_4]^T$ is the state vector and $\boldsymbol{C} \in \mathbb{R}^{1\times 4}$ is the output matrix. Table 1 summarizes parameters η, matrices $\boldsymbol{C}$ and the corresponding

ECG signal generated by the nonlinear oscillator (2). For more details about this model and its parameters, we refer readers to [33]. In order to construct a Takagi-Sugeno fuzzy model, state-space representation (2) is rewritten as follows

$$\dot{\boldsymbol{x}} = \tau \begin{bmatrix} 1 - z_1(x_2) & -1 & 0 & 0 \\ \eta + z_1(x_2) & -7 & 0 & 4 \\ 0 & 0 & 1 - z_2(x_4) & -1 \\ 0 & 8 & \eta + z_2(x_4) & -11 \end{bmatrix} \boldsymbol{x}, \tag{3}$$

with $z_1(x_2) \equiv 1.35x_2 + x_2^2$ and $z_2(x_4) \equiv 1.35x_4 + x_4^2$ being the premise variables. The next step is to use the sector nonlinearity approach [34] to construct a fuzzy model that exactly represents the ECG nonlinear oscillator within a local sector. In order to express the premise variables as a fuzzy blending, we define them as

$$z_1(x_2) = \overline{z_1}\mu_{11}(x_2) + \underline{z_1}\mu_{12}(x_2),$$
$$z_2(x_4) = \overline{z_2}\mu_{21}(x_4) + \underline{z_2}\mu_{22}(x_4).$$

Here, $\mu_{ij}(\cdot) \geq$ are membership functions satisfying

$$\mu_{11}(x_2) + \mu_{12}(x_2) = 1, \quad \mu_{21}(x_4) + \mu_{22}(x_4) = 1,$$

and, within the local sectors $x_2 \in [-10, 10]$ and $x_4 \in [-10, 10]$, the maximum and minimum values of the premise variables are given by

$$\overline{z_1} = \max_{x_2 \in [-10,10]} z_1(x_2) = 113.5,$$
$$\underline{z_1} = \min_{x_2 \in [-10,10]} z_1(x_2) = -0.455625,$$
$$\overline{z_2} = \max_{x_4 \in [-10,10]} z_2(x_4) = 113.5,$$
$$\underline{z_2} = \min_{x_4 \in [-10,10]} z_2(x_4) = -0.455625.$$

Therefore,

$$\mu_{11}(x_2) = \frac{z_1(x_2) - \underline{z_1}}{\overline{z_1} - \underline{z_1}}, \quad \mu_{12}(x_2) = 1 - \mu_{11}(x_2),$$
$$\mu_{21}(x_4) = \frac{z_2(x_4) - \underline{z_2}}{\overline{z_2} - \underline{z_2}}, \quad \mu_{22}(x_4) = 1 - \mu_{21}(x_4).$$

Finally, nonlinear system (2) can be represented by the four-rule Takagi-Sugeno fuzzy model

$$\dot{\boldsymbol{x}} = \tau \sum_{i=1}^{4} h_i(\boldsymbol{x}) \boldsymbol{A}_i \boldsymbol{x}, \tag{4}$$

with the following state matrices $\boldsymbol{A}_i$

$$\boldsymbol{A}_1 = \begin{bmatrix} 1 - \overline{z_1} & -1 & 0 & 0 \\ \eta + \overline{z_1} & -7 & 0 & 4 \\ 0 & 0 & 1 - \overline{z_2} & -1 \\ 0 & 8 & \eta + \overline{z_2} & -11 \end{bmatrix},$$

$$\boldsymbol{A}_2 = \begin{bmatrix} 1 - \overline{z_1} & -1 & 0 & 0 \\ \eta + \overline{z_1} & -7 & 0 & 4 \\ 0 & 0 & 1 - \underline{z_2} & -1 \\ 0 & 8 & \eta + \underline{z_2} & -11 \end{bmatrix},$$

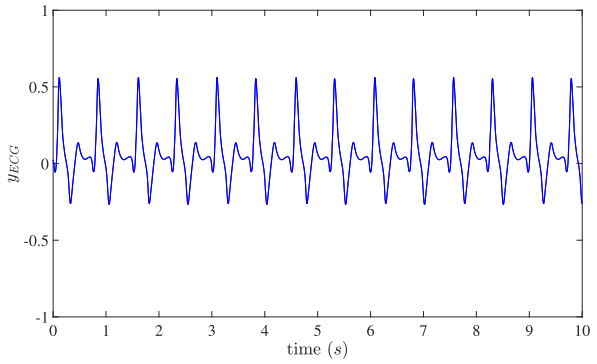

FIGURE 1. ECG signal for a normal heartbeat generated by the Takagi-Sugeno fuzzy model (4) using the parameters summarized in Table 1.

TABLE 1. Some synthetic ECG signals and their corresponding tuning parameter η and matrix $\boldsymbol{C}$.

ECG signal	Parameters
Normal rhythm	$\eta = 3$, $\boldsymbol{C} = [-0.024 \;\; 0.0216 \;\; -0.0012 \;\; 0.12]$.
Sinus tachycardia	$\eta = 2.848$, $\boldsymbol{C} = [0 \;\; -0.1 \;\; 0 \;\; 0]$.
Atrial flutter	$\eta = 2.52$, $\boldsymbol{C} = [-0.068 \;\; 0.028 \;\; -0.024 \;\; 0.12]$.
Ventricular tachycardia	$\eta = 2.178$, $\boldsymbol{C} = [0 \;\; 0 \;\; 0 \;\; -0.1]$.
Ventricular flutter	$\eta = 2.178$, $\boldsymbol{C} = [0.1 \;\; -0.02 \;\; -0.01 \;\; 0]$.

$$\boldsymbol{A}_3 = \begin{bmatrix} 1 - \underline{z_1} & -1 & 0 & 0 \\ \eta + \underline{z_1} & -7 & 0 & 4 \\ 0 & 0 & 1 - \overline{z_2} & -1 \\ 0 & 8 & \eta + \overline{z_2} & -11 \end{bmatrix},$$

$$\boldsymbol{A}_4 = \begin{bmatrix} 1 - \underline{z_1} & -1 & 0 & 0 \\ \eta + \underline{z_1} & -7 & 0 & 4 \\ 0 & 0 & 1 - \underline{z_2} & -1 \\ 0 & 8 & \eta + \underline{z_2} & -11 \end{bmatrix},$$

and the membership functions for the defuzzification process become

$$h_1(\boldsymbol{x}) = \mu_{11}(x_2)\mu_{21}(x_4), \quad h_2(\boldsymbol{x}) = \mu_{11}(x_2)\mu_{22}(x_4),$$
$$h_3(\boldsymbol{x}) = \mu_{12}(x_2)\mu_{21}(x_4), \quad h_4(\boldsymbol{x}) = \mu_{12}(x_2)\mu_{22}(x_4), \tag{5}$$

which also satisfy the property $\sum_{i=1}^{4} h_i(\boldsymbol{x}) = 1$. Figure 1 depicts a waveform generated by the Takagi-Sugeno fuzzy model (4) that corresponds to a normal heartbeat pattern. On the other hand, Figure 2 illustrates waveforms made by the Takagi-Sugeno fuzzy model (4) for four typical irregular heartbeats.

IV. MODEL-BASED TRACKING CONTROL

This section presents LMI conditions for the model-based tracking problem of two ECG nonlinear oscillators represented as Takagi-Sugeno fuzzy models. To this end, we assume that all the states are measurables. Consider the following forced system

$$\dot{\boldsymbol{x}} = \tau \sum_{i=1}^{4} h_i(\boldsymbol{x})(\boldsymbol{A}_i + \boldsymbol{A}_\eta)\boldsymbol{x} + \tau \boldsymbol{B}\boldsymbol{u}. \tag{6}$$

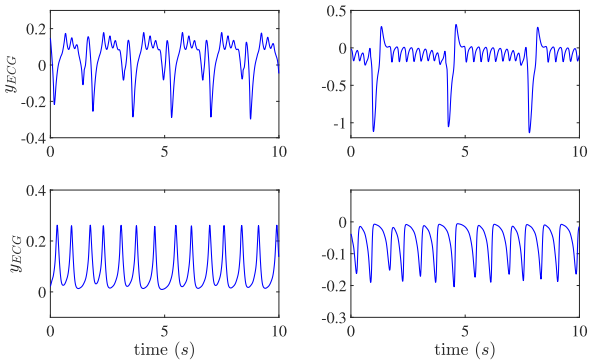

FIGURE 2. ECG signals generated by the Takagi-Sugeno fuzzy model (4) using the parameters summarized in Table 1. Clockwise from top left: sinus tachycardia, atrial flutter, ventricular flutter, and ventricular tachycardia.

In the same way as [27], this proposal uses a multiple input control with matrix $\boldsymbol{B} = \boldsymbol{I}$ and $\boldsymbol{u} = [u_1\ u_2\ u_3\ u_4]^T$. Moreover, $\boldsymbol{A}_\eta \in \mathbb{R}^{4\times4}$ is a mismatching matrix expressed as follows

$$\boldsymbol{A}_\eta = \begin{bmatrix} 0 & 0 & 0 & 0 \\ \delta_\eta & 0 & 0 & 0 \\ 0 & 0 & 0 & 0 \\ 0 & 0 & \delta_\eta & 0 \end{bmatrix}.$$

On the other hand, the reference model is given below.

$$\dot{\boldsymbol{x}}_r = \tau \sum_{i=1}^{4} h_i(\boldsymbol{x}_r)\boldsymbol{A}_i\boldsymbol{x}_r, \tag{7}$$

with $\boldsymbol{x}_r \in \mathbb{R}^{4\times1}$ being the reference state vector. Note that matrices $\boldsymbol{A}_i$ in both the reference (7) and forced (6) systems share the same parameter η, and the inclusion of the mismatching matrix $\boldsymbol{A}_\eta$ in (6) makes the tuning parameter be $\eta + \delta_\eta$. Furthermore, membership functions $h_i(\boldsymbol{x}_r)$ take the same form as in (5), with the difference that they depend on the state vector $\boldsymbol{x}_r$. The purpose of the tracking control problem is to design a PDC control law of the form

$$\boldsymbol{u} = \boldsymbol{v} - \sum_{i=1}^{4} h_i(\boldsymbol{x}_r)\boldsymbol{F}_i\boldsymbol{e}_r. \tag{8}$$

Here, $\boldsymbol{F}_i \in \mathbb{R}^{4\times4}$ and $\boldsymbol{e}_r = \boldsymbol{x} - \boldsymbol{x}_r$. The former term on the right-hand side in the previous equation can be seen as a nominal controller that compensates for the mismatch between the slave system (system to be controlled) (6) and the master (reference model) (7), while the latter matrices will asymptotically stabilize the origin of the following tracking error system

$$\begin{aligned}
\dot{\boldsymbol{e}}_r &= \tau \sum_{i=1}^{4} h_i(\boldsymbol{x})(\boldsymbol{A}_i + \boldsymbol{A}_\eta)\boldsymbol{x} + \tau\boldsymbol{B}\boldsymbol{u} - \tau \sum_{i=1}^{4} h_i(\boldsymbol{x}_r)\boldsymbol{A}_i\boldsymbol{x}_r \\
&= \tau \sum_{i=1}^{4} h_i(\boldsymbol{x})\boldsymbol{A}_i\boldsymbol{x} + \tau\boldsymbol{A}_\eta\boldsymbol{x} + \tau\boldsymbol{B}\boldsymbol{u} - \tau \sum_{i=1}^{4} h_i(\boldsymbol{x}_r)\boldsymbol{A}_i\boldsymbol{x}_r \\
&\quad + \tau \sum_{i=1}^{4} h_i(\boldsymbol{x}_r)\boldsymbol{A}_i\boldsymbol{x} - \tau \sum_{i=1}^{4} h_i(\boldsymbol{x}_r)\boldsymbol{A}_i\boldsymbol{x} \\
&= \tau \sum_{i=1}^{4} h_i(\boldsymbol{x}_r)\boldsymbol{A}_i(\boldsymbol{x} - \boldsymbol{x}_r) + \tau\boldsymbol{A}_\eta\boldsymbol{x} + \tau\boldsymbol{B}\boldsymbol{u} \\
&\quad + \tau \sum_{i=1}^{4} \big(h_i(\boldsymbol{x}) - h_i(\boldsymbol{x}_r)\big)\boldsymbol{A}_i\boldsymbol{x} \\
&= \tau \sum_{i=1}^{4} h_i(\boldsymbol{x}_r)(\boldsymbol{A}_i\boldsymbol{e}_r + \boldsymbol{A}_\eta\boldsymbol{x}) + \tau\boldsymbol{B}\boldsymbol{u} + \boldsymbol{w}_r,
\end{aligned} \tag{9}$$

where

$$\boldsymbol{w}_r = \tau \sum_{i=1}^{4} \big(h_i(\boldsymbol{x}) - h_i(\boldsymbol{x}_r)\big)\boldsymbol{A}_i\boldsymbol{x}.$$

Note that the mismatching term $\boldsymbol{w}_r$ can be regarded as a disturbance [38] that vanishes as $\big(h_i(\boldsymbol{x}) - h_i(\boldsymbol{x}_r)\big) \to 0$ at $t \to \infty$ when using the feedback control law (8). Therefore, the goal is to design a controller that not only stabilizes the zero equilibrium of the error dynamics (9) but also mitigates the effect of the disturbance $\boldsymbol{w}_r$ in an $\mathcal{L}_2$-norm fashion, that is to say,

$$\int_0^{t_f} \boldsymbol{e}_r^T\boldsymbol{e}_r dt \le \gamma^2 \int_0^{t_f} \boldsymbol{w}_r^T\boldsymbol{w}_r dt. \tag{10}$$

Theorem 1: The origin of the tracking error system (9) is asymptotically stable if, for a given $\gamma > 0$, there exist a vector $\boldsymbol{v} \in \mathbb{R}^{4\times1}$, a 4×4 symmetric matrix $\boldsymbol{X} > \boldsymbol{0}$ and matrices $\boldsymbol{M}_1$, $\boldsymbol{M}_2$, $\boldsymbol{M}_3$, $\boldsymbol{M}_4 \in \mathbb{R}^{4\times4}$ such that the following conditions

$$\begin{bmatrix} -\tau(\boldsymbol{A}_i\boldsymbol{X} - \boldsymbol{B}\boldsymbol{M}_i + \boldsymbol{X}\boldsymbol{A}_i^T - \boldsymbol{M}_i^T\boldsymbol{B}^T) & -\boldsymbol{I} & \boldsymbol{X} \\ -\boldsymbol{I} & \gamma^2\boldsymbol{I} & \boldsymbol{0} \\ \boldsymbol{X} & \boldsymbol{0} & \boldsymbol{I} \end{bmatrix} > \boldsymbol{0}, \tag{11}$$

hold true for all $i \in \{1, 2, 3, 4\}$. Moreover, the PDC controller (8) with $\boldsymbol{F}_i = \boldsymbol{M}_i\boldsymbol{X}^{-1}$ renders the $\mathcal{L}_2$ gain of the tracking error system less or equal than γ at $\boldsymbol{w}_r \neq \boldsymbol{0}$.

Proof: The substitution of $\boldsymbol{u}$ given by (8) in (9) leads to the expression

$$\dot{\boldsymbol{e}}_r = \tau \sum_{i=1}^{4} h_i(\boldsymbol{x}_r)\Big\{\big(\boldsymbol{A}_i - \boldsymbol{B}\boldsymbol{F}_i\big)\boldsymbol{e}_r + \boldsymbol{A}_\eta\boldsymbol{x} + \boldsymbol{B}\boldsymbol{v}\Big\} + \boldsymbol{w}_r. \tag{12}$$

Consider a quadratic Lyapunov function $V(\boldsymbol{e}_r) = \boldsymbol{e}_r^T\boldsymbol{P}\boldsymbol{e}_r$, whose time derivative along the trajectories must satisfy the inequality below to meet the performance (10).

$$\begin{aligned}
&-\tau \sum_{i=1}^{4} h_i(\boldsymbol{x}_r)\Big\{\boldsymbol{e}_r^T\boldsymbol{P}\Big[\big(\boldsymbol{A}_i - \boldsymbol{B}\boldsymbol{F}_i\big)\boldsymbol{e}_r + \boldsymbol{A}_\eta\boldsymbol{x} + \boldsymbol{B}\boldsymbol{v}\Big] \\
&\quad + \Big[\boldsymbol{e}_r^T\big(\boldsymbol{A}_i - \boldsymbol{B}\boldsymbol{F}_i\big)^T + \boldsymbol{x}^T\boldsymbol{A}_\eta^T + \boldsymbol{v}^T\boldsymbol{B}^T\Big]\boldsymbol{P}\boldsymbol{e}_r\Big\} \\
&\quad - \boldsymbol{e}_r^T\boldsymbol{P}\boldsymbol{w}_r - \boldsymbol{w}_r^T\boldsymbol{P}\boldsymbol{e}_r - \boldsymbol{e}_r^T\boldsymbol{e}_r + \gamma^2\boldsymbol{w}_r^T\boldsymbol{w}_r \ge 0.
\end{aligned} \tag{13}$$

Since $\boldsymbol{B}$ is invertible, the mismatching term $\boldsymbol{A}_\eta$ can be cancelled by

$$\boldsymbol{v} = -\boldsymbol{B}^{-1}\boldsymbol{A}_\eta\boldsymbol{x}. \tag{14}$$

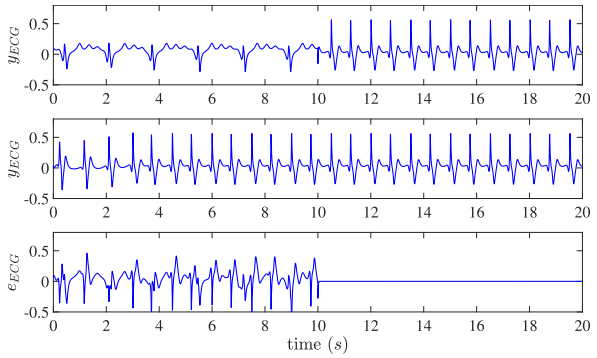

FIGURE 3. Time evolution of the control result with the PDC law (8) acting at $t > 10$. From top to bottom: ECG signal (sinus tachycardia) of the slave system, reference signal, and error (difference of the actual ECG and reference signals).

Hence, obtaining the inequality below.

$$-\tau\sum_{i=1}^{4}h_i(\boldsymbol{x}_r)\Big\{\boldsymbol{e}_r^T\boldsymbol{P}(\boldsymbol{A}_i-\boldsymbol{B}\boldsymbol{F}_i)\boldsymbol{e}_r + \boldsymbol{e}_r^T(\boldsymbol{A}_i^T-\boldsymbol{F}_i^T\boldsymbol{B}^T)\boldsymbol{P}\boldsymbol{e}_r\Big\} - \boldsymbol{e}_r^T\boldsymbol{P}\boldsymbol{w}_r-\boldsymbol{w}_r^T\boldsymbol{P}\boldsymbol{e}_r - \boldsymbol{e}_r^T\boldsymbol{e}_r+\gamma^2\boldsymbol{w}_r^T\boldsymbol{w}_r\geq 0, \tag{15}$$

which can be written in a matrix form as follows

$$\begin{bmatrix}\boldsymbol{e}_r^T & \boldsymbol{w}_r^T\end{bmatrix}\begin{bmatrix}-\tau\sum_{i=1}^{4}h_i(\boldsymbol{x}_r)\boldsymbol{\Omega}_i-\boldsymbol{I} & -\boldsymbol{P}\\ -\boldsymbol{P} & \gamma^2\boldsymbol{I}\end{bmatrix}\begin{bmatrix}\boldsymbol{e}_r\\ \boldsymbol{w}_r\end{bmatrix}\geq 0, \tag{16}$$

with $\boldsymbol{\Omega}_i=\boldsymbol{P}(\boldsymbol{A}_i-\boldsymbol{B}\boldsymbol{F}_i)+(\boldsymbol{A}_i-\boldsymbol{B}\boldsymbol{F}_i)^T\boldsymbol{P}$. Previous inequality reduces to the problem of checking the positivity of the inner matrix $\forall i\in\{1,2,3,4\}$. Matrix multiplication below converts bilinear terms into linear ones.

$$\begin{bmatrix}\boldsymbol{P}^{-1} & 0\\ 0 & \boldsymbol{I}\end{bmatrix}\begin{bmatrix}-\boldsymbol{\Omega}_i-\boldsymbol{I} & -\boldsymbol{P}\\ -\boldsymbol{P} & \gamma^2\boldsymbol{I}\end{bmatrix}\begin{bmatrix}\boldsymbol{P}^{-1} & 0\\ 0 & \boldsymbol{I}\end{bmatrix}, \tag{17}$$

which is equal to

$$\begin{bmatrix}-\tau(\boldsymbol{A}_i\boldsymbol{X}-\boldsymbol{B}\boldsymbol{M}_i+\boldsymbol{X}\boldsymbol{A}_i^T-\boldsymbol{M}_i\boldsymbol{B}^T)-\boldsymbol{X}^2 & -\boldsymbol{I}\\ -\boldsymbol{I} & \gamma^2\boldsymbol{I}\end{bmatrix}, \tag{18}$$

when defining $\boldsymbol{X}=\boldsymbol{P}^{-1}$ and $\boldsymbol{M}_i=\boldsymbol{F}_i\boldsymbol{P}^{-1}$. The application of the Schur complement to convert $\boldsymbol{X}^2$ into linear terms brings the final expression given by (11), completing the proof. ■

Corollary 1: When the mismatching term $\boldsymbol{A}_\eta=\boldsymbol{0}$, the tracking problem (9) reduces to the synchronization problem of two identical oscillators. Thus, PDC control law (8) becomes

$$\boldsymbol{u}=-\sum_{i=1}^{4}h_i(\boldsymbol{x}_r)\boldsymbol{F}_i\boldsymbol{e}_r. \tag{19}$$

A. EXAMPLE

In this subsection, an illustrative example will verify our proposed model-based tracking control conditions for the ECG nonlinear oscillator. In order to calculate the feedback gains matrices, the tuning parameter is set to $\eta=3$, which corresponds to the normal heartbeat, in both the slave (6) and master (7) systems. As for the mismatching matrix $\boldsymbol{A}_\eta$ in (6), $\delta_\eta=-0.152$ is set. It is important to note that by using this setting, the tuning parameter in the state matrices $\boldsymbol{A}_i+\boldsymbol{A}_\eta$ of the slave system (6) becomes $\eta=2.848$, which corresponds to the parameter that generates a sinus tachycardia signal. Therefore, we used the vector $\boldsymbol{C}$ for the sinus tachycardia in the slave system, and the vector $\boldsymbol{C}$ for the normal rhythm in the reference model (see Table 1). LMI conditions in Theorem 1 were feasible with the following matrix $\boldsymbol{X}$

$$\boldsymbol{X}=\begin{bmatrix}1.2558 & 0.0670 & -0.0188 & -0.0561\\ 0.0670 & 3.2172 & -0.0590 & 0.4017\\ -0.0188 & -0.0590 & 1.2765 & 0.1010\\ -0.0561 & 0.4017 & 0.1010 & 3.1010\end{bmatrix},$$

and feedback gains matrices $\boldsymbol{F}_i$

$$\boldsymbol{F}_1=\begin{bmatrix}-73.9849 & 22.9868 & 1.9229 & -3.6366\\ 53.2478 & 11.1942 & 2.8962 & 2.5186\\ 1.8514 & -3.7518 & -75.3314 & 24.3878\\ 2.8571 & 2.7428 & 51.4754 & 9.0461\end{bmatrix},$$

$$\boldsymbol{F}_2=\begin{bmatrix}-73.9775 & 22.9238 & 1.0604 & -3.2589\\ 53.2709 & 10.9961 & 0.1977 & 3.7000\\ 1.3525 & 0.5897 & 40.6248 & -1.5296\\ 2.8123 & 3.0671 & -0.7483 & 7.0324\end{bmatrix},$$

$$\boldsymbol{F}_3=\begin{bmatrix}41.1970 & -0.9669 & 1.3488 & 0.5518\\ -0.5326 & 9.9364 & 2.8603 & 2.7243\\ 0.9863 & -3.3969 & -75.3227 & 24.3260\\ 0.2856 & 3.7971 & 51.5011 & 8.8613\end{bmatrix},$$

$$\boldsymbol{F}_4=\begin{bmatrix}41.2044 & -1.0300 & 0.4863 & 0.9296\\ -0.5096 & 9.7385 & 0.1620 & 3.9054\\ 0.4875 & 0.9446 & 40.6334 & -1.5915\\ 0.2410 & 4.1210 & -0.7227 & 6.8477\end{bmatrix}. \tag{20}$$

Figure 3 shows the simulation result of the tracking control applied to the ECG nonlinear oscillator. The simulation starts with an open-loop configuration, therefore, the slave system is generating an ECG signal that resembles a sinus tachycardia waveform. Starting at $t=10\,s.$, the PDC control law (8) with (14) and the feedback matrices (20) acts to achieve tracking of the normal heartbeat signal. In order to evaluate the difference of the ECG output signals, we have switched the vector $\boldsymbol{C}$ of the slave system to the one for the normal heartbeat for $t>10\,s$. Figure 4 depicts the states of both the slave and the reference systems, the tracking error, and the control input signals $\boldsymbol{u}=[u_1\ u_2\ u_3\ u_4]^T$.

V. ROBUST TRACKING OF THE ECG NONLINEAR OSCILLATOR

A pillar of Theorem 1 is the cancellation of the mismatching matrix $\boldsymbol{A}_\eta$ by the feedback controller. Note that a variation on the parameter δ_η might compromise the stability of the closed-loop system. For this reason, the present section deals with the tracking control of a Takagi-Sugeno fuzzy ECG

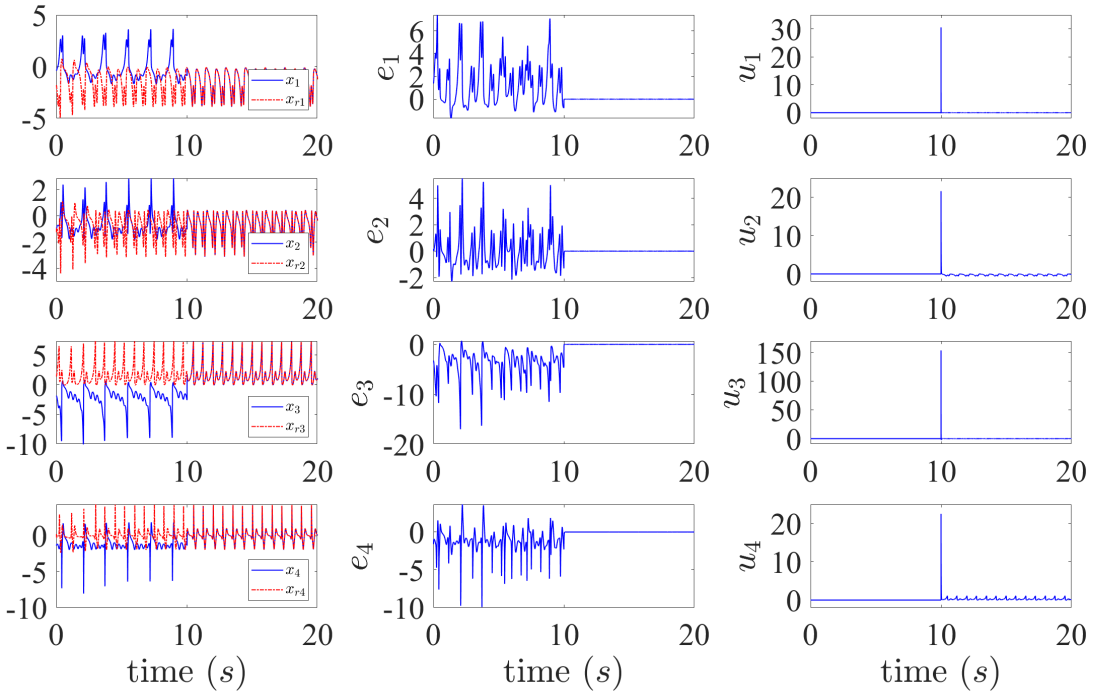

FIGURE 4. Time evolution of the control result with the PDC law (8) acting at $t > 10$. Left column: states of the slave system (solid blue line) and master system (dashed-dotted red line). Center column: tracking error $e_r = x - x_r$. Right Column: control inputs.

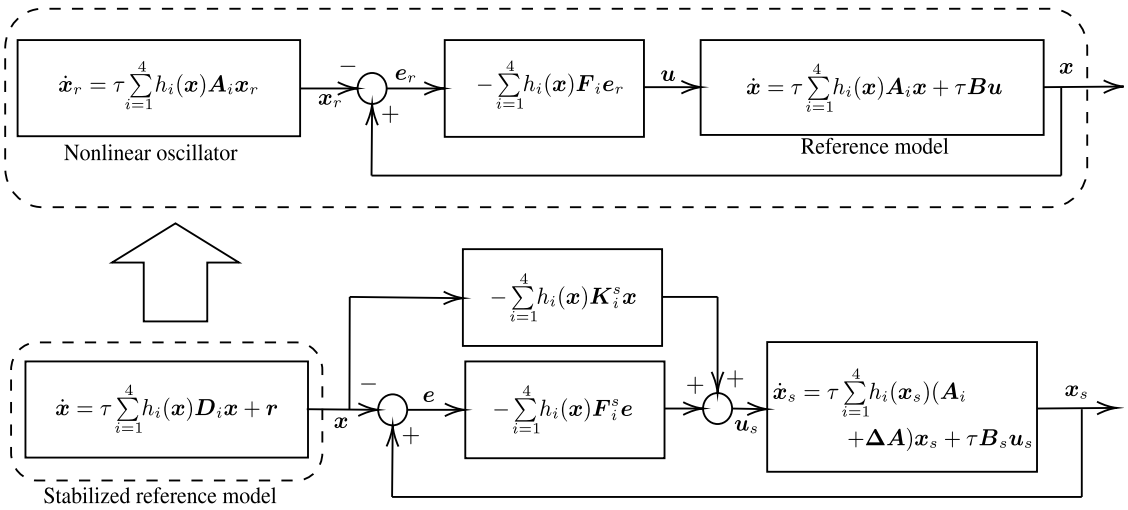

FIGURE 5. Block diagram of the overall robust tracking control scheme in Theorem 2.

oscillator with uncertainties given as

$$\dot{\boldsymbol{x}}_s = \tau \sum_{i=1}^{4} h_i(\boldsymbol{x}_s)(\boldsymbol{A}_i + \boldsymbol{\Delta A})\boldsymbol{x}_s + \tau \boldsymbol{B}_s \boldsymbol{u}_s. \tag{21}$$

Here $\boldsymbol{\Delta A} = \Delta_\eta \boldsymbol{\mathcal{X}}_1^T \boldsymbol{\mathcal{Y}}_1 + \Delta_\eta \boldsymbol{\mathcal{X}}_2^T \boldsymbol{\mathcal{Y}}_2$ is the matrix of uncertainties and $\boldsymbol{\mathcal{X}}_1 = [0\ 1\ 0\ 0]$, $\boldsymbol{\mathcal{Y}}_1 = [1\ 0\ 0\ 0]$, $\boldsymbol{\mathcal{X}}_2 = [0\ 0\ 0\ 1]$, $\boldsymbol{\mathcal{Y}}_2 = [0\ 0\ 1\ 0]$. Note that this configuration includes uncertainty in the tuning parameter expressed as $\eta + \Delta\eta$. Furthermore, the uncertainty satisfies the norm-bounded constraint $|\Delta_\eta| < \phi$, where ϕ is the upper bound. Similar to other approaches to designing a model-based reference tracking control (see [38], [39], [40], [41], [42] and references therein), a stable reference model is required. However, matrices $\boldsymbol{A}_2$, $\boldsymbol{A}_3$ and $\boldsymbol{A}_4$ in the Takagi-Sugeno fuzzy model (4) at $\eta = 3$ possess at least one positive eigenvalue, and therefore, the system is unstable. Whereas the approaches in [38], [39], and [42] use an arbitrary chosen stable reference system $\boldsymbol{\mathcal{R}} = \sum_{i=1}^{z_r} \boldsymbol{A}_i \boldsymbol{x} + \boldsymbol{r}$ to track the reference input $\boldsymbol{r}$, note that in our scheme shown in Fig. 5, system (7) generates

a reference signal and using Theorem 1, both (6) and (7) systems are synchronized resulting in the feedback stabilized Takagi-Sugeno fuzzy system below.

$$\dot{\boldsymbol{x}} = \tau \sum_{i=1}^{4} h_i(\boldsymbol{x}) \boldsymbol{D}_i \boldsymbol{x} + \boldsymbol{r}, \tag{22}$$

where $\boldsymbol{D}_i = \boldsymbol{A}_i - \boldsymbol{B}\boldsymbol{F}_i$ and $\boldsymbol{r} = \tau \sum_{i=1}^{4} h_i(\boldsymbol{x}) \boldsymbol{B}\boldsymbol{F}_i \boldsymbol{x}_r$. For the sake of simplicity, feedback gain vectors $\boldsymbol{F}_i$ are calculated for a PDC law (19) that stabilizes the equilibrium of the error dynamics (9) of two identical oscillators with $\eta = 3$ (that is to say, $\boldsymbol{A}_\eta = \boldsymbol{0}$) and sharing the same membership functions. Next, the control law to achieve robust tracking is given as follows

$$\boldsymbol{u}_s = -\sum_{i=1}^{4} h_i(\boldsymbol{x}) \{\boldsymbol{F}_i^s \boldsymbol{e} + \boldsymbol{K}_i^s \boldsymbol{x}\}. \tag{23}$$

With this in mind, the error equation $\boldsymbol{e} = \boldsymbol{x}_s - \boldsymbol{x}$ leads to the following dynamics

$$\begin{aligned} \dot{\boldsymbol{e}} &= \tau \sum_{i=1}^{4} h_i(\boldsymbol{x}) \Big\{ \big(\boldsymbol{A}_i + \boldsymbol{\Delta A}\big)\boldsymbol{x}_s - \boldsymbol{D}_i \boldsymbol{x} - \boldsymbol{B}_s \boldsymbol{F}_i^s \boldsymbol{e} \\ &\quad - \boldsymbol{B}_s \boldsymbol{K}_i^s \boldsymbol{x} \Big\} + \boldsymbol{w} - \boldsymbol{r}, \\ &= \tau \sum_{i=1}^{4} h_i(\boldsymbol{x}) \Big\{ \big(\boldsymbol{A}_i + \boldsymbol{\Delta A} - \boldsymbol{B}_s \boldsymbol{F}_i^s\big)\boldsymbol{e} + \big(\boldsymbol{A}_i + \boldsymbol{\Delta A} \\ &\quad - \boldsymbol{D}_i - \boldsymbol{B}_s \boldsymbol{K}_i^s\big)\boldsymbol{x} \Big\} + \boldsymbol{w} - \boldsymbol{r}. \end{aligned} \tag{24}$$

In the same way as in Section IV, the disparity term $\boldsymbol{w} = \tau \sum_{i=1}^{4} \big(h_i(\boldsymbol{x}_s) - h_i(\boldsymbol{x})\big)\boldsymbol{A}_i \boldsymbol{x}_s$ will be seen as a disturbance. Expressing (24) as an augmented system gives

$$\dot{\boldsymbol{e}}_s = \tau \sum_{i=1}^{4} h_i(\boldsymbol{x})(\boldsymbol{\Lambda}_i + \boldsymbol{\Delta\Lambda})\boldsymbol{e}_s + \boldsymbol{E}\boldsymbol{w}_s. \tag{25}$$

Here,

$$\boldsymbol{\Lambda}_i = \begin{bmatrix} \boldsymbol{A}_i - \boldsymbol{B}_s \boldsymbol{F}_i^s & \boldsymbol{A}_i - \boldsymbol{D}_i - \boldsymbol{B}_s \boldsymbol{K}_i^s \\ \boldsymbol{0} & \boldsymbol{D}_i \end{bmatrix},$$
$$\boldsymbol{\Delta\Lambda} = \begin{bmatrix} \boldsymbol{\Delta A} & \boldsymbol{\Delta A} \\ \boldsymbol{0} & \boldsymbol{0} \end{bmatrix},$$
$$\boldsymbol{e}_s = \begin{bmatrix} \boldsymbol{e} \\ \boldsymbol{x} \end{bmatrix}, \ \boldsymbol{E} = \begin{bmatrix} \boldsymbol{I} & -\boldsymbol{I} \\ \boldsymbol{0} & \boldsymbol{I} \end{bmatrix}, \ \boldsymbol{w}_s = \begin{bmatrix} \boldsymbol{w} \\ \boldsymbol{r} \end{bmatrix}.$$

Given this setting, the theorem below will provide conditions to guarantee that the tracking error dynamics (25) will be stable even in the presence of variations on the tuning parameter η as long as they are within the norm-bounded constraint.

Theorem 2: The zero equilibrium of the tracking error system (25) is asymptotically stable if, for a given $\gamma > 0$ and $|\Delta_\eta| < \phi$, there exist a symmetric matrix $\boldsymbol{\Psi} = diag(\boldsymbol{\Psi}_1, \boldsymbol{\Psi}_2) > \boldsymbol{0}$, matrices $\boldsymbol{M}_1^s, \boldsymbol{M}_2^s, \boldsymbol{M}_3^s, \boldsymbol{M}_4^s, \boldsymbol{N}_1^s, \boldsymbol{N}_2^s, \boldsymbol{N}_3^s, \boldsymbol{N}_4^s \in \mathbb{R}^{4\times 4}$, a matrix $\boldsymbol{G} \in \mathbb{R}^{8\times 8}$ and $\alpha < 0$ such that LMI conditions (26) and (27) are feasible for all $i \in \{1, 2, 3, 4\}$.

$$\begin{bmatrix} -\tau \mathscr{H}\{\boldsymbol{\Lambda}_i^{\Psi}\} - \tau \boldsymbol{G} & -\boldsymbol{E} & \boldsymbol{\Psi} \\ * & \gamma^2 \boldsymbol{I} & \boldsymbol{0} \\ * & * & \boldsymbol{I} \end{bmatrix} > \boldsymbol{0}, \tag{26}$$

$$\begin{bmatrix} \boldsymbol{G} - \phi^2 \boldsymbol{\mathcal{X}} & \boldsymbol{\Psi}_1 \boldsymbol{\mathcal{Y}}_1^T & \boldsymbol{\Psi}_1 \boldsymbol{\mathcal{Y}}_2^T \\ & \boldsymbol{\Psi}_2 \boldsymbol{\mathcal{Y}}_1^T & \boldsymbol{\Psi}_2 \boldsymbol{\mathcal{Y}}_2^T \\ * * & \boldsymbol{I} & \boldsymbol{0} \\ * * & * & \boldsymbol{I} \end{bmatrix} \geq \boldsymbol{0}. \tag{27}$$

Then the synchronization vectors become $\boldsymbol{F}_i^s = \boldsymbol{M}_i^s \boldsymbol{\Psi}_1^{-1}$ and $\boldsymbol{K}_i^s = \boldsymbol{N}_i^s \boldsymbol{\Psi}_2^{-1}$.

Proof: In this proof, we leverage a quadratic Lyapunov function of the form $V(\boldsymbol{e}_s) = \boldsymbol{e}_s^T \boldsymbol{\Psi}^{-1} \boldsymbol{e}_s$ where $\boldsymbol{\Psi}^{-1} = diag(\boldsymbol{\Psi}_1^{-1}, \boldsymbol{\Psi}_2^{-1})$ and $\boldsymbol{\Psi}_1^{-1}, \ \boldsymbol{\Psi}_2^{-1} \in \mathbb{R}^{4\times 4}$ are symmetric matrices. Here, we aim at designing a controller that not only stabilizes the equilibrium but also mitigates the discrepancy of the two models expressed as the disturbance $\boldsymbol{w}_s$ in an $\mathcal{L}_2$-norm fashion. Therefore, the time derivative along the trajectories of the Lyapunov function candidate must satisfy the inequality below.

$$\begin{aligned} &\tau \sum_{i=1}^{4} h_i(\boldsymbol{x}) \boldsymbol{e}_s^T \big\{ \boldsymbol{\Psi}^{-1}(\boldsymbol{\Lambda}_i + \boldsymbol{\Delta\Lambda}) + (\boldsymbol{\Lambda}_i + \boldsymbol{\Delta\Lambda})^T \boldsymbol{\Psi}^{-1} \big\} \boldsymbol{e}_s \\ &\quad + \boldsymbol{e}_s^T \boldsymbol{\Psi}^{-1} \boldsymbol{E} \boldsymbol{w}_s + \boldsymbol{w}_s^T \boldsymbol{E}^T \boldsymbol{\Psi}^{-1} \boldsymbol{e}_s + \boldsymbol{e}_s^T \boldsymbol{e}_s - \gamma^2 \boldsymbol{w}_s^T \boldsymbol{w}_s \leq \boldsymbol{0}. \end{aligned} \tag{28}$$

Previous inequality can be rewritten in the following matrix form

$$\begin{aligned} &\sum_{i=1}^{4} h_i(\boldsymbol{x}) \begin{bmatrix} \boldsymbol{e}_s \\ \boldsymbol{w}_s \end{bmatrix}^T \\ &\times \begin{bmatrix} \tau \mathscr{H}\big\{\boldsymbol{\Psi}^{-1}(\boldsymbol{\Lambda}_i + \boldsymbol{\Delta\Lambda})\big\} + \boldsymbol{I} & \boldsymbol{\Psi}^{-1}\boldsymbol{E} \\ * & -\gamma^2 \boldsymbol{I} \end{bmatrix} \begin{bmatrix} \boldsymbol{e}_s \\ \boldsymbol{w}_s \end{bmatrix} \leq \boldsymbol{0}. \end{aligned} \tag{29}$$

From now on, the notation $\mathscr{H}\{\boldsymbol{\chi}\} = \boldsymbol{\chi} + \boldsymbol{\chi}^T$ is adopted, and the asterisk signifies the transpose operation on the respective symmetric entry. Since condition (29) involves a single fuzzy summation, it is required to test for positive definiteness of the inner matrices for all $i =\in \{1, 2, 3, 4\}$ to guarantee the satisfaction of previous inequality. Therefore

$$\begin{bmatrix} -\tau \mathscr{H}\big\{\boldsymbol{\Psi}^{-1}\boldsymbol{\Lambda}_i + \boldsymbol{\Psi}^{-1}\boldsymbol{\Delta\Lambda}\big\} - \boldsymbol{I} & -\boldsymbol{\Psi}^{-1}\boldsymbol{E} \\ * & \gamma^2 \boldsymbol{I} \end{bmatrix} \geq \boldsymbol{0}, \tag{30}$$

multiplying both sides by $diag(\boldsymbol{\Psi}, \boldsymbol{I})$ gives

$$\begin{bmatrix} -\tau \mathscr{H}\big\{\boldsymbol{\Lambda}_i \boldsymbol{\Psi} + \boldsymbol{\Delta\Lambda\Psi}\big\} - \boldsymbol{\Psi}^2 & -\boldsymbol{E} \\ * & \gamma^2 \boldsymbol{I} \end{bmatrix} \geq \boldsymbol{0}, \tag{31}$$

which is converted into the convex condition below thanks to the Schur complement.

$$\begin{bmatrix} -\tau \mathscr{H}\big\{\boldsymbol{\Lambda}_i^{\Psi} + \boldsymbol{\Delta\Lambda}^{\Psi}\big\} & -\boldsymbol{E} & \boldsymbol{\Psi} \\ * & \gamma^2 \boldsymbol{I} & \boldsymbol{0} \\ * & * & \boldsymbol{I} \end{bmatrix} \geq \boldsymbol{0}, \tag{32}$$

where

$$\boldsymbol{\Lambda}_i^{\Psi} = \begin{bmatrix} \boldsymbol{A}_i\boldsymbol{\Psi}_1 - \boldsymbol{B}_s\boldsymbol{M}_i^s & \boldsymbol{A}_i\boldsymbol{\Psi}_2 - \boldsymbol{D}_i\boldsymbol{\Psi}_2 - \boldsymbol{B}_s\boldsymbol{N}_i^s \\ \boldsymbol{0} & \boldsymbol{D}_i\boldsymbol{\Psi}_2 \end{bmatrix},$$
$$\boldsymbol{\Delta\Lambda}^{\Psi} = \begin{bmatrix} \boldsymbol{\Delta A}\boldsymbol{\Psi}_1 & \boldsymbol{\Delta A}\boldsymbol{\Psi}_2 \\ \boldsymbol{0} & \boldsymbol{0} \end{bmatrix}. \tag{33}$$

Rewriting inequality (32) as follows

$$\begin{bmatrix} -\tau\mathscr{H}\{\boldsymbol{\Lambda}_i^{\Psi}\} & -\boldsymbol{E}^{\Psi} & \boldsymbol{\Psi} \\ * & \gamma^2\boldsymbol{I} & \boldsymbol{0} \\ * & * & \boldsymbol{I} \end{bmatrix} - \begin{bmatrix} \tau\mathscr{H}\{\boldsymbol{\Delta\Lambda}^{\Psi}\} & \boldsymbol{0} & \boldsymbol{0} \\ * & \boldsymbol{0} & \boldsymbol{0} \\ * & * & \boldsymbol{0} \end{bmatrix} \geq \boldsymbol{0}. \tag{34}$$

Hence,

$$\mathscr{H}\{\boldsymbol{\Delta\Lambda}^{\Psi}\} = \mathscr{H}\left\{ \begin{bmatrix} \Delta_\eta\boldsymbol{\mathcal{X}}_1^T \\ \boldsymbol{0} \end{bmatrix} [\boldsymbol{\mathcal{Y}}_1\boldsymbol{\Psi}_1 \ \boldsymbol{\mathcal{Y}}_1\boldsymbol{\Psi}_2] + \begin{bmatrix} \Delta_\eta\boldsymbol{\mathcal{X}}_2^T \\ \boldsymbol{0} \end{bmatrix} [\boldsymbol{\mathcal{Y}}_2\boldsymbol{\Psi}_1 \ \boldsymbol{\mathcal{Y}}_2\boldsymbol{\Psi}_2] \right\}. \tag{35}$$

After the application of Young's inequality, it yields

$$\begin{aligned} \mathscr{H}\{\boldsymbol{\Delta\Lambda}^{\Psi}\} &\leq \Delta_\eta\Delta_\eta^T \begin{bmatrix} \boldsymbol{\mathcal{X}}_1^T \\ \boldsymbol{0} \end{bmatrix} [\boldsymbol{\mathcal{X}}_1 \ \boldsymbol{0}] \\ &\quad + \Delta_\eta\Delta_\eta^T \begin{bmatrix} \boldsymbol{\mathcal{X}}_2^T \\ \boldsymbol{0} \end{bmatrix} [\boldsymbol{\mathcal{X}}_2 \ \boldsymbol{0}] \\ &\quad + \begin{bmatrix} \boldsymbol{\Psi}_1\boldsymbol{\mathcal{Y}}_1^T \\ \boldsymbol{\Psi}_2\boldsymbol{\mathcal{Y}}_1^T \end{bmatrix} [\boldsymbol{\mathcal{Y}}_1\boldsymbol{\Psi}_1 \ \boldsymbol{\mathcal{Y}}_1\boldsymbol{\Psi}_2] \\ &\quad + \begin{bmatrix} \boldsymbol{\Psi}_1\boldsymbol{\mathcal{Y}}_2^T \\ \boldsymbol{\Psi}_2\boldsymbol{\mathcal{Y}}_2^T \end{bmatrix} [\boldsymbol{\mathcal{Y}}_2\boldsymbol{\Psi}_1 \ \boldsymbol{\mathcal{Y}}_2\boldsymbol{\Psi}_2] \\ &\leq \begin{bmatrix} \boldsymbol{\Psi}_1\boldsymbol{\mathcal{Y}}_1^T \\ \boldsymbol{\Psi}_2\boldsymbol{\mathcal{Y}}_1^T \end{bmatrix} [\boldsymbol{\mathcal{Y}}_1\boldsymbol{\Psi}_1 \ \boldsymbol{\mathcal{Y}}_1\boldsymbol{\Psi}_2] \\ &\quad + \begin{bmatrix} \boldsymbol{\Psi}_1\boldsymbol{\mathcal{Y}}_2^T \\ \boldsymbol{\Psi}_2\boldsymbol{\mathcal{Y}}_2^T \end{bmatrix} [\boldsymbol{\mathcal{Y}}_2\boldsymbol{\Psi}_1 \ \boldsymbol{\mathcal{Y}}_2\boldsymbol{\Psi}_2] + \phi^2\boldsymbol{\mathcal{X}}, \end{aligned} \tag{36}$$

with $\Delta_\eta\Delta_\eta^T \leq \phi^2$ and

$$\boldsymbol{\mathcal{X}} = \begin{bmatrix} \boldsymbol{\mathcal{X}}_1^T \\ \boldsymbol{0} \end{bmatrix} [\boldsymbol{\mathcal{X}}_1 \ \boldsymbol{0}] + \begin{bmatrix} \boldsymbol{\mathcal{X}}_2^T \\ \boldsymbol{0} \end{bmatrix} [\boldsymbol{\mathcal{X}}_2 \ \boldsymbol{0}]. \tag{37}$$

As a relaxation tool [43], we introduce a symmetric matrix $\boldsymbol{G}$ that meets the inequality below.

$$\boldsymbol{G} - \phi^2\boldsymbol{\mathcal{X}} - \begin{bmatrix} \boldsymbol{\Psi}_1\boldsymbol{\mathcal{Y}}_1^T \\ \boldsymbol{\Psi}_2\boldsymbol{\mathcal{Y}}_1^T \end{bmatrix} [\boldsymbol{\mathcal{Y}}_1\boldsymbol{\Psi}_1 \ \boldsymbol{\mathcal{Y}}_1\boldsymbol{\Psi}_2] + \begin{bmatrix} \boldsymbol{\Psi}_1\boldsymbol{\mathcal{Y}}_2^T \\ \boldsymbol{\Psi}_2\boldsymbol{\mathcal{Y}}_2^T \end{bmatrix} [\boldsymbol{\mathcal{Y}}_2\boldsymbol{\Psi}_1 \ \boldsymbol{\mathcal{Y}}_2\boldsymbol{\Psi}_2] \geq \boldsymbol{0}, \tag{38}$$

which can be transformed into a linear condition using the Schur complement, leading to the condition (27). Finally

$$\begin{bmatrix} -\tau\mathscr{H}\{\boldsymbol{\Lambda}_i^{\Psi}\} - \tau\mathscr{H}\{\boldsymbol{\Delta\Lambda}^{\Psi}\} & -\boldsymbol{E}^{\Psi} & \boldsymbol{\Psi} \\ * & \gamma\boldsymbol{I} & \boldsymbol{0} \\ * & * & \gamma\boldsymbol{I} \end{bmatrix} \geq \begin{bmatrix} -\tau\mathscr{H}\{\boldsymbol{\Lambda}_i^{\Psi}\} - \tau\boldsymbol{G} & -\boldsymbol{E}^{\Psi} & \boldsymbol{\Psi} \\ * & \gamma\boldsymbol{I} & \boldsymbol{0} \\ * & * & \gamma\boldsymbol{I} \end{bmatrix} > \boldsymbol{0}. \tag{39}$$

Thus, this completes the proof. ■

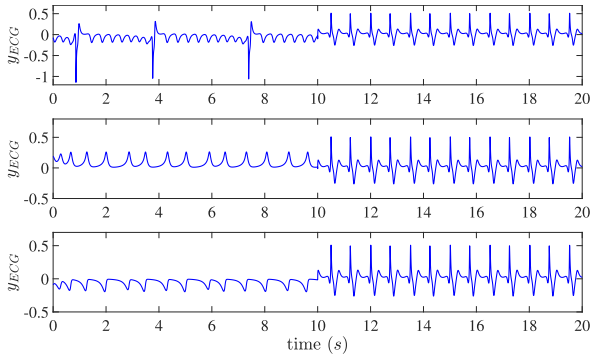

FIGURE 6. Time evolution of the control result with the PDC law (23) acting at $t > 10$. From top to bottom: atrial flutter, ventricular tachycardia, and ventricular flutter.

Remark 1: Note that conditions in Theorem 2 are infeasible if the reference model is not stable. This fact can be demonstrated from (32). Such inequality holds true if the leading principal matrix $-\tau\mathscr{H}\{\boldsymbol{\Lambda}_i^{\Psi} + \boldsymbol{\Delta\Lambda}^{\Psi}\}$ is positive definite [44]. After applying the Schur complement, it results that $-\left(\tau\boldsymbol{D}_i\boldsymbol{\Psi}_2 + \tau\boldsymbol{\Psi}_2^T\boldsymbol{D}_i\right)^{-1} > \boldsymbol{0}$. Therefore, no matrix $\boldsymbol{\Psi}_2 > \boldsymbol{0}$ exists for Hurwitz unstable matrices $\boldsymbol{D}_i$ [45].

A. EXAMPLE

This subsection uses an example to test the LMI conditions for the tracking problem of a system with uncertainties. Firstly, two identical oscillators were synchronized with $\eta = 3$ by Corollary 1. The matrices computed from the feasible solution are shown below.

$$\boldsymbol{F}_1 = \begin{bmatrix} -15.9017 & 12.1813 & 3.1258 & -0.2290 \\ 57.3039 & 13.9682 & 9.1387 & 2.0499 \\ 2.9002 & -0.0972 & -18.6787 & 11.3502 \\ 8.3063 & 2.4562 & 51.2844 & 11.0632 \end{bmatrix},$$

$$\boldsymbol{F}_2 = \begin{bmatrix} -15.8838 & 12.1433 & 2.3042 & -0.0420 \\ 57.3905 & 13.6135 & 1.9598 & 3.6824 \\ 2.4856 & 2.7668 & 89.5897 & -0.9896 \\ 8.1797 & 2.4180 & -1.3650 & 10.7383 \end{bmatrix},$$

$$\boldsymbol{F}_3 = \begin{bmatrix} 91.6433 & 0.8991 & 2.4866 & 2.3410 \\ 0.1160 & 14.5034 & 9.0873 & 1.8189 \\ 2.0733 & 0.0839 & -18.6575 & 11.3152 \\ 1.6677 & 3.8816 & 51.3961 & 10.7680 \end{bmatrix},$$

$$\boldsymbol{F}_4 = \begin{bmatrix} 91.6519 & 0.8625 & 1.7090 & 2.5131 \\ 0.1991 & 14.1470 & 1.8313 & 3.4738 \\ 1.7022 & 2.9311 & 89.6020 & -1.0235 \\ 1.4754 & 3.8649 & -1.2587 & 10.4428 \end{bmatrix}.$$

Consequently, the control system (22) becomes stable. The next step is to calculate the feedback gains matrices, to do so, let us set $\eta = 3$, $\boldsymbol{B}_s = \boldsymbol{I}$ and $\Delta_\eta = -0.882$ implying that $\phi^2 = 0.676$. It is worth mentioning that this Δ_η covers all the different values of η stated in Table 1. The solutions for

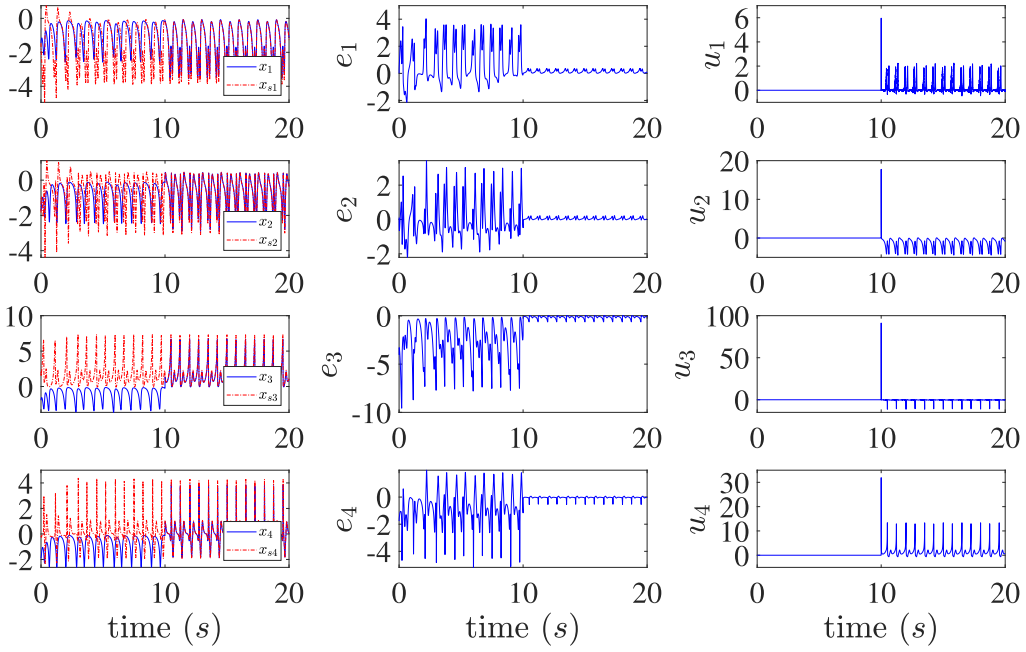

FIGURE 7. Time evolution of the control result with the PDC law (23) acting at $t > 10$. Left column: states of the slave system at $\eta = 2.178$ (solid blue line) and reference system (dashed-dotted red line). Center column: tracking error $e = x_s - x$. Right column: control inputs.

Theorem 2 are given by

$$\boldsymbol{\Psi}_1 = \begin{bmatrix} 2.5428 & 0.0451 & 0.0113 & -0.0159 \\ 0.0451 & 3.2580 & -0.0066 & 0.1361 \\ 0.0113 & -0.0066 & 2.5798 & 0.0524 \\ -0.0159 & 0.1361 & 0.0524 & 3.2209 \end{bmatrix},$$

$$\boldsymbol{\Psi}_2 = \begin{bmatrix} 2.4746 & -0.3797 & 0.0004 & -0.2936 \\ -0.3797 & 10.1289 & -0.3052 & 1.2633 \\ 0.0004 & -0.3052 & 2.5196 & -0.2270 \\ -0.2936 & 1.2633 & -0.2270 & 10.6051 \end{bmatrix},$$

the matrices $\boldsymbol{F}_i^s$, $\boldsymbol{K}_i^s$ and $\boldsymbol{G}$ are as shown in the equation at the top of the next page,

$$\boldsymbol{F}_1^s = \begin{bmatrix} 3.6377 & 19.2354 & 0.1049 & 1.5238 \\ 15.5412 & 45.0849 & 0.5123 & 5.4943 \\ 0.0502 & 1.3535 & 3.6242 & 18.0721 \\ 0.5017 & 5.4571 & 15.0631 & 41.4109 \end{bmatrix},$$

$$\boldsymbol{F}_2^s = \begin{bmatrix} 3.0031 & 19.2893 & 0.3181 & 1.0660 \\ 15.6093 & 44.8612 & 0.8417 & 4.9667 \\ 0.5887 & 0.8264 & 51.8755 & -0.6056 \\ 0.1196 & 4.3968 & -0.9214 & 27.6843 \end{bmatrix},$$

$$\boldsymbol{F}_3^s = \begin{bmatrix} 52.3208 & -0.2419 & 0.6133 & 0.8210 \\ -0.5512 & 30.0239 & 0.1529 & 4.5805 \\ 0.2771 & 0.9691 & 3.0254 & 18.1473 \\ 0.8494 & 5.0597 & 15.1471 & 41.2216 \end{bmatrix},$$

$$\boldsymbol{F}_4^s = \begin{bmatrix} 52.0488 & -0.2560 & 0.3498 & 0.3724 \\ -0.5470 & 29.3206 & 0.4689 & 3.5681 \\ 0.3453 & 0.4211 & 51.6095 & -0.6029 \\ 0.4822 & 3.5096 & -0.9094 & 27.0159 \end{bmatrix},$$

$$\boldsymbol{K}_1^s = \begin{bmatrix} 0.3749 & 1.7717 & 0.2254 & 0.6077 \\ 2.3301 & 4.1656 & 0.4737 & 1.2428 \\ 0.1766 & 0.5041 & 0.2448 & 1.4057 \\ 0.3800 & 1.0722 & 2.1265 & 3.6206 \end{bmatrix},$$

$$\boldsymbol{K}_2^s = \begin{bmatrix} 0.4334 & 1.8293 & -0.0048 & 0.3582 \\ 2.4222 & 4.3252 & -0.0530 & 0.7618 \\ 0.1230 & 0.3527 & 4.4483 & 0.2482 \\ 0.4532 & 0.9098 & -0.2961 & 0.0964 \end{bmatrix},$$

$$\boldsymbol{K}_3^s = \begin{bmatrix} 4.4800 & 0.3213 & 0.1545 & 0.3578 \\ -0.2642 & 0.5816 & 0.5515 & 1.0782 \\ 0.0011 & 0.3405 & 0.2971 & 1.4551 \\ -0.0260 & 0.7404 & 2.2106 & 3.7668 \end{bmatrix},$$

$$\boldsymbol{K}_4^s = \begin{bmatrix} 4.6661 & 0.3133 & 0.0004 & 0.1751 \\ -0.2590 & 0.5894 & 0.0203 & 0.5563 \\ 0.0020 & 0.2092 & 4.6273 & 0.2338 \\ 0.0319 & 0.5329 & -0.2916 & 0.0968 \end{bmatrix}.$$

The tuning parameter of the slave system is firstly set to $\eta = 2.52$ and then to $\eta = 2.178$ for running the simulations. Notice that the former configuration matches with the atrial flutter waveform setting and the latter matches with both the ventricular tachycardia and ventricular flutter setting (see Table 1). Figures 6 illustrates the simulation result of the robust tracking control applied to an ECG nonlinear oscillator with the above configurations. Over the first 10 seconds, the slave system is operating in an open-loop way and the robust tracking controller (23) takes action starting at $t = 10\ s$. For the sake of comparison, we have switched the output vectors $\boldsymbol{C}$ of the slave system to that for the normal heartbeat for $t > 10\ s$. Finally, the states of both the slave system (with $\eta = 2.178$) as well as the reference system, the tracking error,

$$G = \begin{bmatrix} 8.6293 & 0.0246 & 0.1659 & 0.3436 & -7.4473 & 1.0281 & -0.3638 & -0.4755 \\ 0.0246 & 3.2989 & 0.3768 & -0.2200 & -1.3630 & -0.1969 & -0.5344 & -0.1499 \\ 0.1659 & 0.3768 & 8.2581 & -0.1432 & -0.3263 & -0.5419 & -6.8164 & 1.3727 \\ 0.3436 & -0.2200 & -0.1432 & 3.3928 & -0.4533 & -0.1784 & -1.1415 & -0.0261 \\ -7.4473 & -1.3630 & -0.3263 & -0.4533 & 18.3184 & -2.4746 & 0.5690 & 0.9512 \\ 1.0281 & -0.1969 & -0.5419 & -0.1784 & -2.4746 & 1.4768 & 1.0612 & -0.4340 \\ -0.3638 & -0.5344 & -6.8164 & -1.1415 & 0.5690 & 1.0612 & 17.2585 & -3.1545 \\ -0.4755 & -0.1499 & 1.3727 & -0.0261 & 0.9512 & -0.4340 & -3.1545 & 1.6509 \end{bmatrix}.$$

and the output signals are shown in Figure 7 placed at the top of the previous page.

Compared to other works that use multivariable control such as the adaptive scheme to synchronize a pair of identical autonomous cardiac conduction models in [27], and the rate regulation of a bradycardia ECG signal in [28], our approach deals with a model based-tracking control method to restore the dynamics of an uncertain nonlinear oscillator from an abnormal situation (arrhythmia-like waveform) to normal behavior as shown in Figure 6. Some studies focused on the stabilization of unstable periodic orbits (see [23], [24]) have successfully suppressed undesired chaotic behavior that may be associated with cardiac pathologies. The results in [24] show that their method is effective for a specific undesired behavior. On the other hand, this proposal is able to handle a variety of unwanted dynamics within the norm-bounded conditions. Finally, the multiple linear subsystem form of the Takagi-Sugeno fuzzy model allows for a discretization as in [22], with the difference that our method proves the stability of the closed-loop system.

VI. CONCLUSION

In this work, we presented an LMI design procedure for the model-based tracking control for an ECG nonlinear oscillator described in a Takagi-Sugeno fuzzy form. The profile of the synthetic ECG waveform depends on an intrinsic parameter denoted as η. Firstly, the cancellation of the discrepancy between the slave and master systems by a PDC control law to achieve the tracking objective was considered. In a second approach, the assumption that the variation on the parameter η is an uncertainty in the slave system led to a robust tracking control procedure to deal with this problem. Our results demonstrated the effectiveness of the proposed strategies to achieve model-based tracking control for the ECG nonlinear oscillator in both a nominal and an uncertain slave system configuration. This reflects the possibility of suppressing undesirable behaviors in a cardiac model and restoring a normal rhythm by using control techniques. Compared with the methods in [22], [23], [24], [27], and [28], the proposed Takagi-Sugeno fuzzy representation leads to simple LMI design conditions. Moreover, with the inclusion of parametric uncertainty in the tuning parameter η in Theorem 2, the proposed robust tracking controller can deal with a variety of undesired arrhythmias. Despite the fact that the ECG signals are generated by a phenomenological model. This mathematical description leads to the first level of validity and reliability for testing unconventional solutions and opens new ways to gain an understanding of the studied system. We are certain that our work provides significant conceptual proof that could assist in the improvement of cardiac devices. Future work is to obtain a discrete-time Takagi-Sugeno fuzzy model of the system (4) and then derive conditions for the design of a state observer. Note that the nature of discrete-time models will lead to a simple implementation on embedded platforms. A current limitation of our framework is the rate regulation, which represents a different control objective for a follow-up study. Finally, we will address the model-based robust tracking control scheme to a more comprehensive heart model such as those given in [16], [17], and [18].

REFERENCES

[1] *World Health Statistics 2021: Monitoring Health for the SDGs, Sustainable Development Goals*, World Health Organization, Geneva, Switzerland, 2021.

[2] P. F. Cranefield, A. L. Wit, and B. F. Hoffman, "Genesis of cardiac arrhythmias," *Circulation*, vol. 47, no. 1, pp. 190–204, Jan. 1973.

[3] J. P. Keener and J. Sneyd, *Mathematical Physiology: II: Systems Physiology*. Berlin, Germany: Springer, 2008.

[4] R. A. Gray, A. M. Pertsov, and J. Jalife, "Spatial and temporal organization during cardiac fibrillation," *Nature*, vol. 392, no. 6671, pp. 75–78, Mar. 1998.

[5] X.-S. Wu, W. Cai, P. Zhu, and W. Yuan, "New strategies for arrhythmia treatment," *J. Cardiol. Cardiovasc. Theraphy*, vol. 5, no. 1, pp. 756–763, 2018.

[6] C. C. Goodman and K. S. Fuller, *Pathology for the Physical Therapist Assistant*. Amsterdam, The Netherlands: Elsevier, 2012.

[7] N. Clementy, A. Bodin, A. Bisson, A. P. Teixeira-Gomes, S. Roger, D. Angoulvant, V. Labas, and D. Babuty, "The defibrillation conundrum: New insights into the mechanisms of shock-related myocardial injury sustained from a life-saving therapy," *Int. J. Mol. Sci.*, vol. 22, no. 9, pp. 1–17, 2021.

[8] W. Tang, M. H. Weil, S. Sun, D. Jorgenson, C. Morgan, K. Klouche, and D. Snyder, "The effects of biphasic waveform design on post-resuscitation myocardial function," *J. Amer. College Cardiol.*, vol. 43, no. 7, pp. 1228–1235, Apr. 2004.

[9] S. Boccaletti, "The control of chaos: Theory and applications," *Phys. Rep.*, vol. 329, no. 3, pp. 103–197, May 2000.

[10] F. X. Witkowski, K. M. Kavanagh, P. A. Penkoske, R. Plonsey, M. L. Spano, W. L. Ditto, and D. T. Kaplan, "Evidence for determinism in ventricular fibrillation," *Phys. Rev. Lett.*, vol. 75, no. 6, pp. 1230–1233, Aug. 1995.

[11] P. E. McSharry, G. D. Clifford, L. Tarassenko, and L. A. Smith, "A dynamical model for generating synthetic electrocardiogram signals," *IEEE Trans. Biomed. Eng.*, vol. 50, no. 3, pp. 289–294, Mar. 2003.

[12] E. Ryzhii and M. Ryzhii, "A heterogeneous coupled oscillator model for simulation of ECG signals," *Comput. Methods Programs Biomed.*, vol. 117, no. 1, pp. 40–49, Oct. 2014.

[13] M. A. Quiroz-Juárez, R. Vázquez-Medina, E. Ryzhii, M. Ryzhii, and J. L. Aragón, "Quasiperiodicity route to chaos in cardiac conduction model," *Commun. Nonlinear Sci. Numer. Simul.*, vol. 42, pp. 370–378, Jan. 2017.

[14] M. A. Quiroz-Juárez, O. Jiménez-Ramírez, R. Vázquez-Medina, E. Ryzhii, M. Ryzhii, and J. L. Aragón, "Cardiac conduction model for generating 12 lead ECG signals with realistic heart rate dynamics," *IEEE Trans. Nanobiosci.*, vol. 17, no. 4, pp. 525–532, Oct. 2018.
[15] M. A. Quiroz-Juárez, O. Jiménez-Ramírez, J. L. Aragón, J. L. Del Río-Correa, and R. Vázquez-Medina, "Periodically kicked network of RLC oscillators to produce ECG signals," *Comput. Biol. Med.*, vol. 104, pp. 87–96, Jan. 2019.
[16] S. Sovilj, R. Magjarevic, N. H. Lovell, and S. Dokos, "A simplified 3D model of whole heart electrical activity and 12-lead ECG generation," *Comput. Math. Methods Med.*, vol. 2013, pp. 1–10, Apr. 2013.
[17] M. Balakrishnan, V. S. Chakravarthy, and S. Guhathakurta, "Simulation of cardiac arrhythmias using a 2D heterogeneous whole heart model," *Frontiers Physiol.*, vol. 6, p. 374, Dec. 2015.
[18] N. Biasi and A. Tognetti, "Modelling whole heart electrical activity for ischemia and cardiac pacing simulation," *Health Technol.*, vol. 10, no. 4, pp. 837–850, Jul. 2020.
[19] A. Garfinkel, J. N. Weiss, W. L. Ditto, and M. L. Spano, "Chaos control of cardiac arrhythmias," *Trends Cardiovascular Med.*, vol. 5, no. 2, pp. 76–80, Mar. 1995.
[20] M. E. Brandt, H.-T. Shih, and G. Chen, "Linear time-delay feedback control of a pathological rhythm in a cardiac conduction model," *Phys. Rev. E, Stat. Phys. Plasmas Fluids Relat. Interdiscip. Top.*, vol. 56, no. 2, pp. 1334–1337, Aug. 1997.
[21] A. Garfinkel, M. L. Spano, W. L. Ditto, and J. N. Weiss, "Controlling cardiac chaos," *Science*, vol. 257, no. 5074, pp. 1230–1235, Aug. 1992.
[22] M. E. Brandt, G. Wang, and H.-T. Shih, "Feedback control of a nonlinear dual–oscillator heartbeat model," in *Bifurcation Control: Theory and Applications*. Berlin, Germany: Springer, 2003, pp. 265–273.
[23] B. B. Ferreira, A. S. de Paula, and M. A. Savi, "Chaos control applied to heart rhythm dynamics," *Chaos, Solitons Fractals*, vol. 44, no. 8, pp. 587–599, Aug. 2011.
[24] F. Lounis, A. Boukabou, and A. Soukkou, "Implementing high-order chaos control scheme for cardiac conduction model with pathological rhythms," *Chaos Solit. Fractals*, vol. 132, Mar. 2020, Art. no. 109581.
[25] D. J. Christini and J. J. Collins, "Using chaos control and tracking to suppress a pathological nonchaotic rhythm in a cardiac model," *Phys. Rev. E, Stat. Phys. Plasmas Fluids Relat. Interdiscip. Top.*, vol. 53, no. 1, pp. 49–52, Jan. 1996.
[26] F. R. Boroujeni, N. Vasegh, and A. K. Sedigh, "Control of cardiac arrhythmia by nonlinear spatiotemporal delayed feedback," *Int. J. Bifurcation Chaos*, vol. 24, no. 11, Nov. 2014, Art. no. 1450140.
[27] D. Baleanu, S. S. Sajjadi, J. H. Asad, A. Jajarmi, and E. Estiri, "Hyperchaotic behaviors, optimal control, and synchronization of a nonautonomous cardiac conduction system," *Adv. Difference Equ.*, vol. 2021, no. 1, pp. 1–24, Dec. 2021.
[28] M. A. A. Semnani, A. R. Vali, S. M. Hakimi, and V. Behnamgol, "Modelling and design of observer based smooth sliding mode controller for heart rhythm regulation," *Int. J. Dyn. Control*, vol. 10, no. 3, pp. 828–842, Jun. 2022.
[29] M. E. Karar, "Robust RBF neural network-based backstepping controller for implantable cardiac pacemakers," *Int. J. Adapt. Control Signal Process.*, vol. 32, no. 7, pp. 140–1051, 2018.
[30] P. Khan, Y. Khan, and S. Kumar, "Activity-based tracking and stabilization of human heart rate using fuzzy FO-PID controller," *IEEE J. Emerg. Sel. Topics Ind. Electron.*, vol. 3, no. 2, pp. 372–381, Apr. 2022.
[31] S. Momani, I. M. Batiha, and R. El-Khazali, "Design of PI$^{\lambda}$D$^{\delta}$-heart rate controllers for cardiac pacemaker," in *Proc. IEEE Int. Symp. Signal Process. Inf. Technol. (ISSPIT)*, Dec. 2019, pp. 1–5.
[32] W. V. Shi, "Advanced intelligent control of cardiac pacemaker systems using a fuzzy PID controller," *Int. J. Intell. Control Syst.*, vol. 18, no. 2, pp. 28–34, 2013.
[33] M. A. Quiroz-Juárez, O. Jiménez-Ramírez, R. Vázquez-Medina, V. Breña-Medina, J. L. Aragón, and R. A. Barrio, "Generation of ECG signals from a reaction-diffusion model spatially discretized," *Sci. Rep.*, vol. 9, no. 1, pp. 1–10, Dec. 2019.
[34] T. Taniguchi, K. Tanaka, H. Ohtake, and H. O. Wang, "Model construction, rule reduction, and robust compensation for generalized form of Takagi–Sugeno fuzzy systems," *IEEE Trans. Fuzzy Syst.*, vol. 9, no. 4, pp. 525–538, Aug. 2001.
[35] K. Tanaka and H. O. Wang, *Fuzzy Control Systems Design and Analysis: A Linear Matrix Inequality Approach*. Hoboken, NJ, USA: Wiley, 2001.
[36] S. Boyd, L. E. Ghaoui, E. Feron, and V. Balakrishnan, *Linear Matrix Inequalities in System and Control Theory*. Philadelphia, PA, USA: SIAM, 1994.
[37] R. James Caverly and J. Richard Forbes, "LMI properties and applications in systems, stability, and control theory," 2019, *arXiv:1903.08599*.
[38] S. Bezzaoucha, B. Marx, D. Maquin, and J. Ragot, "Model reference tracking control for nonlinear systems described by Takagi–Sugeno structure," in *Proc. IEEE Int. Conf. Fuzzy Syst. (FUZZ-IEEE)*, Jul. 2013, pp. 1–8.
[39] B. Mansouri, N. Manamanni, K. Guelton, A. Kruszewski, and T. Guerra, "Output feedback LMI tracking control conditions with H_∞ criterion for uncertain and disturbed T–S models," *Inf. Sci.*, pp. 446–457, Oct. 2008.
[40] L. Fu, H. K. Lam, F. Liu, B. Xiao, and Z. Zhong, "Static output-feedback tracking control for positive polynomial fuzzy systems," *IEEE Trans. Fuzzy Syst.*, vol. 30, no. 6, pp. 1722–1733, Jun. 2022.
[41] Y. Yu, H. Lam, and K. Y. Chan, "T–S fuzzy-model-based output feedback tracking control with control input saturation," *IEEE Trans. Fuzzy Syst.*, vol. 26, no. 6, pp. 3514–3523, Dec. 2018.
[42] B. Xiao, H.-K. Lam, H. Zhou, and J. Gao, "Analysis and design of interval type-2 polynomial-fuzzy-model-based networked tracking control systems," *IEEE Trans. Fuzzy Syst.*, vol. 29, no. 9, pp. 2750–2759, Sep. 2021.
[43] K. Tanaka, M. Tanaka, Y. Chen, and H. O. Wang, "A new sum-of-squares design framework for robust control of polynomial fuzzy systems with uncertainties," *IEEE Trans. Fuzzy Syst.*, vol. 24, no. 1, pp. 94–110, Feb. 2016.
[44] T. Lyche, *Numerical Linear Algebra and Matrix Factorizations*. Cham, Switzerland: Springer, 2020.
[45] G.-R. Duan and R. J. Patton, "A note on Hurwitz stability of matrices," *Automatica*, vol. 34, no. 4, pp. 509–511, Apr. 1998.

JAIRO MORENO-SÁENZ (Member, IEEE) received the B.Eng. degree in communication and electronic engineering and the M.Sc. degree in microelectronic engineering from the National Polytechnic Institute (IPN), Mexico City, Mexico, in 2012 and 2015, respectively, and the Ph.D. degree from The University of Electro-Communications, Tokyo, Japan, in 2020. He is currently a Postdoctoral Fellow with the Department of Mechanical and Intelligent Systems Engineering, The University of Electro-Communications, and an Adjunct Professor with Escuela de Ingeniería y Ciencias, Tecnológico de Monterrey, Mexico City. His research interests include linear and nonlinear control, systems identification, and reinforcement learning.

YING-JEN CHEN (Member, IEEE) received the B.S. degree in electrical engineering from National Taiwan Ocean University, Keelung, Taiwan, in 2002, the M.S. degree in electrical engineering from the Lunghwa University of Science and Technology, Taoyuan City, Taiwan, in 2004, and the Ph.D. degree in electrical engineering from National Central University, Taoyuan City, in 2011.

He was a Postdoctoral Researcher with the Department of Mechanical Engineering and Intelligent Systems, The University of Electro-Communications, Tokyo, Japan, from 2012 to 2014. He was a Project Manager with the Research and Development Department, CTCI Advanced Systems Inc., from 2014 to 2015. He was an Assistant Professor with the Department of Electrical Engineering, National Taipei University, Taiwan, from 2015 to 2022. He is currently an Assistant Professor with the Department of Electrical Engineering, Yuan Ze University, Taoyuan City. His current research interests include fuzzy control systems, computer vision, and robotics.

Dr. Chen received the Outstanding Youth Award from the Taiwan Fuzzy Systems Association, in 2021, the First Prize Paper Award from the Proceedings of the International Conference on Applied System Innovation (ICASI), Sapporo, Japan, in 2017, and the Best Paper Award from the Proceedings of the IEEE International Conference on Control System, Computing and Engineering (ICCSCE), Penang, Malaysia, in 2013.

KAZUO TANAKA (Fellow, IEEE) received the B.S. and M.S. degrees in electrical engineering from Hosei University, Tokyo, Japan, in 1985 and 1987, respectively, and the Ph.D. degree in systems science from the Tokyo Institute of Technology, in 1990.

He was a Visiting Scientist in computer science with the University of North Carolina at Chapel Hill, in 1992 and 1993. He is currently a Professor with the Department of Mechanical and Intelligent Systems Engineering, The University of Electro-Communications. His research interests include intelligent systems and control, nonlinear systems control, and their applications to unmanned aerial vehicles.

Dr. Tanaka is a fellow of IFSA. He was a recipient of the 2021 Fuzzy Systems Pioneer Award from the IEEE Computational Intelligence Society. He received the Best Young Researchers Award from the Japan Society for Fuzzy Theory and Systems, in 1990, the Outstanding Papers Award from the 1990 Annual NAFIPS Meeting in Toronto, Canada, in 1990, the Outstanding Papers Award from the Joint Hungarian-Japanese Symposium on Fuzzy Systems and Applications in Budapest, Hungary, in 1991, the Best Young Researchers Award from the Japan Society for Mechanical Engineers, in 1994, the Outstanding Book Awards from the Japan Society for Fuzzy Theory and Systems, in 1995, the1999 IFAC World Congress Best Poster Paper Prize, in 1999, the 2000 IEEE TRANSACTIONS ON FUZZY SYSTEMS Outstanding Paper Award, in 2000, the Best Paper Selection from the 2005 American Control Conference in Portland, USA, in 2005, the Best Paper Award from the 2013 IEEE International Conference on Control System, Computing and Engineering in Penang, Malaysia, in 2013, the Best Paper Finalist from the 2013 International Conference on Fuzzy Theory and Its Applications, Taipei, Taiwan, in 2013, the Best Poster Award, The First International Symposium on Swarm Behavior and Bio-Inspired Robotics (SWARM 2015), Kyoto, Japan, in 2015, and the Robotics Society of Japan Distinguished Service Award, in 2016. He served as an Associate Editor for *Automatica* and the IEEE TRANSACTIONS ON FUZZY SYSTEMS. He is also serving as an Associate Editor for the IEEE Control Systems Society Conference Editorial Board.

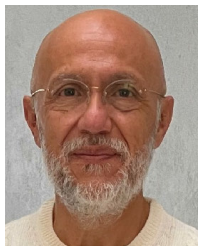

JOSÉ LUIS ARAGÓN received the M.Sc. degree in physics from the National Autonomous University of Mexico (UNAM), in 1988, and the Ph.D. degree in materials physics from Centro de Investigación Científica y de Educación Superior de Ensenada, Mexico, in 1990. He is currently a Full Professor with the Center for Applied Physics and Advanced Technology, UNAM. His research projects include several topics from mathematical biology, to wave propagation in aperiodic structures, and Clifford algebras.

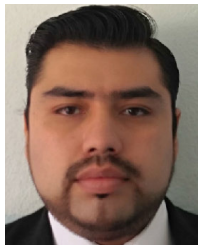

MARIO ALAN QUIROZ-JUÁREZ received the B.S. degree in electronic engineering with a control concentration, the M.Sc. degree in microelectronic specializing in analysis, control e implementation of dynamic systems, and the Ph.D. degree in communications and electronics from Escuela de Ingeniería Mecánica y Eléctrica Unidad Culhúacan (ESIME UC), National Polytechnic Institute (IPN), in 2011 and 2014. He is currently an Associate Professor with the Center for Applied Physics and Advanced Technology, National Autonomous University of Mexico. His research interests include machine learning, artificial intelligence, analysis of biological systems, and the development of hardware for different applications.